https://dx.doi.org/10.1016/j.jsv.2018.02.064

Selection of regularization parameter for l_1-regularized damage detection

Rongrong Hou[1], Yong Xia[1*], Yuequan Bao[2], and Xiaoqing Zhou[3]

[1]*Department of Civil and Environmental Engineering, The Hong Kong Polytechnic University, Kowloon, Hong Kong, China*

[2]*School of Civil Engineering, Harbin Institute of Technology, China*

[3]*College of Civil Engineering, Shenzhen University, China*

*Corresponding author, email: ceyxia@polyu.edu.hk

Abstract

The l_1 regularization technique has been developed for structural health monitoring and damage detection through employing the sparsity condition of structural damage. The regularization parameter, which controls the trade-off between data fidelity and solution size of the regularization problem, exerts a crucial effect on the solution. However, the l_1 regularization problem has no closed-form solution, and the regularization parameter is usually selected by experience. This study proposes two strategies of selecting the regularization parameter for the l_1-regularized damage detection problem. The first method utilizes the residual and solution norms of the optimization problem and ensures that they are both small. The other method is based on the discrepancy principle, which requires that the variance of the discrepancy between the calculated and measured responses is close to the variance of the measurement noise. The two methods are applied to a cantilever beam and a

three-story frame. A range of the regularization parameter, rather than one single value, can be determined. When the regularization parameter in this range is selected, the damage can be accurately identified even for multiple damage scenarios. This range also indicates the sensitivity degree of the damage identification problem to the regularization parameter.

Keywords

Damage detection, sparsity, l_1 regularization, regularization parameter, vibration method

1. Introduction

Vibration-based damage detection has received considerable attention in the past decades [1–3]. Finite element (FE) model updating can locate and quantify damage by utilizing structural vibration properties, such as natural frequencies and mode shapes [4–7].

The identification of structural damage based on measured modal parameters is essentially an inverse problem in mathematics and is typically ill-posed because of the large condition number of the sensitivity matrix [8]. Therefore, measurement noise would lead to inaccurate damage identification. In this regard, the regularization technique is employed by including a regularization term in the objective function, such that a physically meaningful and stable solution can be obtained [8]. Moreover, sensitivity-based model updating is underdetermined in the presence of infinite solutions because of the less number of identifiable modal parameters than that of structural elements. In this situation, the regularization technique is also required to obtain a unique solution.

Tikhonov regularization, also known as l_2 regularization, is a most commonly used scheme to stabilize the inverse problem and has been widely used in structural damage detection [9, 10]. l_2 regularization has a closed-form solution and is thus efficient and convenient for implementation. However, this method tends to produce over-smooth solutions because the quadratic regularizer cannot recover the sharp features of the solution. Consequently, damage identification results are usually distributed to many structural elements, most of which are falsely identified as damage [11–13]. Similar results have also been reported in signal and visual reconstruction [14].

Civil structures generally contain a large number of elements or components whereas damage usually occurs at several sections or members only. Therefore, the damage index is zero for most elements, except for damaged ones. The damage index can be regarded as a sparse vector. According to sparse recovery theory, the l_1 regularization technique can effectively solve inverse problems, which possess sparsity in time or spatial domain [15]. This theory was initially employed in seismology and verified to perform better in preserving isolated characteristics than l_2 norm regularization [16]. Sparse recovery theory has gained substantial attention in the recent years for compressive sensing (CS) and has been widely applied in signal processing, wireless sensing, and image reconstruction [17, 18]. This theory has also been applied to structural health monitoring (SHM) [19–22]. In particular, Zhou *et al*. [23] proposed a damage identification method by combining substructure-based sensitivity analysis and l_1 sparse regularization. Zhou *et al.* [11] developed a new damage detection method based on sparse recovery theory by using frequency data only. l_1 regularization was employed in FE model updating to improve the damage identifiability. The technique was later extended by including frequency and mode shapes [13]. Zhang *et al*. [24] presented a time-domain damage detection algorithm using the extended Kalman filter technique; l_1 regularization was imposed in the optimization process to suppress the interference of measurement noise and improve

the identification accuracy.

In regularization methods, the regularization parameter plays a critical role by trading off the size of the regularized solution and how well it fits the given data [25]. A well-balanced regularization parameter can effectively deal with the ill-posedness of the inverse problem and yield a meaningful and stable solution. A number of methods have been developed to determine the optimal regularization parameter for inverse problems in mathematics; these methods include discrepancy principle (DP) [26-28], ordinary and generalized cross validations (GCV) [29], universal rules [30], and min–max rules [31]. The l_2 regularization has the closed-form solution; as such, tractable methods can be used to choose the regularization parameters [32], such as the widely used L-curve criterion [33]. However, the selection criterion of the regularization parameter for the l_1 regularization problem is very limited because the problem has no closed-form solution.

In SHM, an appropriate regularization parameter for the l_1-regularized problem is problem-dependent and typically selected by experience. Mascarenas *et al*. [34] set the regularization parameter as unit heuristically. Yang and Nagarajaiah [35] reported the insensitivity of the solution to the regularization parameter and set it as 0.01 in CS-based modal identification. Another study [36] calculated the regularization parameter using $\beta = 1/\sqrt{N}$ (where N is the number of the time history sampling points corresponding to the dimension of the unknown vector). Zhang and Xu [12] chose the regularization parameter by using the re-weighted l_1 regularization technique. Yao *et al*. [37] showed that the plot of the residual term versus the regularization term on the linear scale resembled an "L" shape; afterward, they selected the regularization parameter corresponding to the corner of the L curve.

In this study, two strategies are developed for selecting the regularization parameter for the l_1-regularized problem. Inspired by the L-curve criterion used in the l_2

regularization, the first strategy utilizes the residual and solution norms of the optimization problem to determine an appropriate range of the regularization parameter for the problem. The second strategy is based on the DP used in the l_2 counterpart. The two techniques yield consistent results. Their effectiveness is demonstrated through applications to a laboratory tested cantilever beam and a steel frame.

2. Sensitivity-based Damage Detection using l_1 Regularization

In structural damage identification, the global stiffness matrix of an undamaged structure can be expressed as follows [2, 11]

$$[K] = \sum_{i=1}^{n} \alpha_i \left[K^i\right] \tag{1}$$

where $\left[K^i\right]$ is the ith element stiffness matrix, α_i is the element stiffness parameter, and n is the number of elements. Under the assumption that only the element stiffness is reduced when damage occurs, the structural stiffness matrix in the damaged state takes the following form

$$[K] = \sum_{i=1}^{n} (1 + p_i) \left[K^i\right] \tag{2}$$

where p_i is the stiffness reduction factor (SRF) and defined as [11, 38]

$$p_i = \frac{\tilde{\alpha}_i - \alpha_i}{\alpha_i} \tag{3}$$

where $\tilde{\alpha}_i$ is the element stiffness parameter in the damaged state. SRF indicates both the damage location and damage severity.

The relationship between the changes in the modal parameters $\{\Delta R\}$ and damage parameters $\{p\}$ can be expressed as

$$[\mathrm{S}]\{p\} = \{\Delta R\} = \{R^E\} - \{R^0\} \tag{4}$$

where $\{R^E\}$ and $\{R^0\}$ are the measured and analytical modal parameters, respectively; and $[\mathrm{S}]$ is the sensitivity matrix of the modal data with respect to the damage parameter and can be calculated using the FE model of the structure.

As mentioned previously, the inverse problem in Eq. (4) is typically ill-posed and underdetermined. $\{p\}$ is a sparse vector of which only several items are non-zero because only a small number of elements are damaged compared with the total elements in the entire structure. Therefore, the l_1 regularization technique is employed to regularize the inverse problem mentioned above. The damage identification accuracy can be improved by utilizing the sparsity of structural damage as prior information. Damage parameter $\{p\}$ can thus be obtained by solving the following optimization problem

$$\hat{p} = \arg\min_{\hat{p}}(\|\{R(p)\} - \{R^E\}\|_2^2 + \beta\|\{p\}\|_1) \tag{5}$$

where $\{R(p)\} = [\mathrm{S}]\{p\} + \{R^0\}$ and $\beta > 0$ is the regularization parameter. $\|\{R(p)\} - \{R^E\}\|_2^2$ is the data-fitting term or residual norm that indicates the fitness of the solution to the data; and $\|\{p\}\|_1$ is the l_1-regularization term or solution norm that quantifies the sparsity of the solution.

In this study, natural frequency and mode shape are utilized in model updating and damage detection. Thus, Eq. (5) can be rewritten as [11, 13]

$$\hat{p} = \arg\min_{\hat{p}} \left(\frac{1}{m}\sum_{i=1}^{m}\left[\frac{\lambda_i^A(\{p\}) - \lambda_i^E}{\lambda_i^E}\right]^2 + \frac{1}{m \times np}\sum_{i=1}^{m}\sum_{j=1}^{np}\left[\phi_{ji}^A(\{p\}) - \phi_{ji}^E\right]^2 + \frac{\beta}{n}\|\{p\}\|_1 \right) \tag{6}$$

where $\{\lambda_i\}$ is the ith eigenvalue, $\{\phi_{ji}\}$ is the ith mode shape at jth point, m is the number of available eigenvalues, np is the number of measurement points, and superscripts "A" and "E" represent the analytical and experimental terms, respectively. The eigenvalue changes of each mode are normalized with respect to the

measurement values. The eigenvalue residual, eigenvector residual, and regularization terms are divided by the length of the vectors (i.e., m, $m \times np$ and n, respectively) to make these terms comparable.

3. Selection Strategies for the Regularization Parameter

Selection of the regularization parameter is a crucial issue for all regularization problems. Many strategies for selection of the regularization parameter have been proposed for l_2 regularization problems; however, few strategies have been established for l_1 regularization problems.

3.1 Parameter selection using residual and solution norms

The regularization parameter controls the trade-off between data fidelity and solution sparsity. The 2-norm of the residue $\|R(\{p\}) - \{R^E\}\|_2^2$ evaluates the data fidelity, and the 1-norm $\|\{p\}\|_1$ measures the sparsity of the solution. Therefore, the residual and solution norms are closely associated with the regularization parameter.

A small regularization parameter will place higher penalty on the residual term and causes the term very small, leading to an overfitting solution. By contrast, for a large regularization parameter, the regularization term $\beta\|\{p\}\|_1$ becomes dominant in the objective function and is more penalized by the optimization algorithm. Consequently, the residual norm increases, and the result losses data fidelity. When the regularization parameter β exceeds the threshold β_{max}, a zero solution is obtained [39]. Therefore, an appropriate regularization parameter β should be between the two extremes to achieve balance between the two norms and obtain a stable and reasonable solution.

In this study, the plots of the residual and solution norms versus the regularization parameter are utilized to determine the appropriate regularization parameter. For a

given damage detection problem, the corresponding objective function is first solved over a range of β. The associated residual and solution norms are calculated and plotted versus the regularization parameter. The solution norm decreases, whereas the residual norm increases with increasing regularization parameter. The parameter keeping both norm values small is thus considered as an appropriate regularization parameter.

3.2 Parameter selection based on DP

The DP has gained wide applications in machine learning and statistics areas for l_2 regularizations. Lukas [40] applied the DP for choosing the regularization parameter in a discrete and probabilistic setting and investigated the asymptotic properties of the estimated regularization parameter. Hämarik and Raus [41] developed the DP for parameter selection of Tikhonov regularization with given error bound of data. Dong *et al.* [42] utilized the DP to choose the regularization parameter for current distribution reconstruction and compared its performance with the L-curve, the GCV, and the quasi-optimality (QO) criteria. It showed that the L-curve criterion performs much worse than DP, GCV, and QO. However, GCV demands enormous computational effort and is not as stable as other parameter selectors. For QO, it is not applicable to iterative and nonlinear regularization problems. When the statistics of the noise can be estimated, the DP is a prime choice since the rationale behind is clear and only the residuals are required to be computed.

The method is developed here for the present l_1-regularized damage detection problem. Considering a standard l_1-regularized problem

$$\hat{x} = \arg\min_{\hat{x}}(\|[\Phi]\{x\} - \{y^E\}\|_2^2 + \beta\|\{x\}\|_1) \tag{7}$$

where $\{y^E\} = \{y\} + \{\varepsilon\} \in R^M$ is the measurement perturbed by noise $\{\varepsilon\}$, and $[\Phi] \in R^{M\times N}$ $(M < N)$ is a linear operator. The unknown desired solution is denoted by $\{\hat{x}\} \in R^N$, which satisfies $[\Phi]\{\hat{x}\} = \{y\}$. Hence,

$$\|[\Phi]\{\hat{x}\} - \{y^E\}\| = \|[\Phi]\{\hat{x}\} - \{y\} - \{\varepsilon\}\| = \|\{\varepsilon\}\| \tag{8}$$

The DP aims to find a regularization parameter $\beta \geq 0$, such that the corresponding solution $\{x_\beta\}$ satisfies the following equation

$$\left\|[\Phi]\{x_\beta\} - \{y^E\}\right\| = \|\{\varepsilon\}\| \tag{9}$$

Forcing $\{y_\beta\}(= [\Phi]\{x_\beta\})$ exactly the same as $\{y^E\}$ is insensible because $\{y^E\}$ contains error. The reproduced $\{y_\beta\}$ should approximate $\{y^E\}$ within the expected value of the error $\{\varepsilon\}$ [26-28].

For the vibration-based damage detection problem, the perturbation $\{\varepsilon\}$ is primarily attributed to the measurement noise of the modal data. According to the DP, the residual of the modal parameter calculated from a proper regularization parameter should match some statistical characteristics of the noise. The DP could be relaxed as follows considering the existence of uncertainties

$$\left|\left\|R_\beta(\{p\}) - \{R^E\}\right\| - \|\{\varepsilon\}\|\right| \leq Tol \tag{10}$$

where $R_\beta(\{p\})$ is the analytical modal parameter calculated from the identified damage state for a particular β, and $\{R^E\}$ is the measured modal parameter.

In this study, the DP will be revised to be suitable to the l_1 regularization problem for damage detection. In practice, the experimentally measured modal data are contaminated by measurement noise; this scenario is generally assumed as a stochastic process [43-45], as shown in the following equation

$$R^E = (1 + \delta\mu)R \tag{11}$$

where R is the true modal parameter without noise, μ is a random variable following the normal distribution with zero mean and unit variance, and δ denotes the noise level. The relative discrepancy between the calculated modal data and the measured ones is expressed by the following equation

$$D = \frac{\{R^E\} - \{R_\beta(p)\}}{\{R_\beta(p)\}} = \delta\mu \tag{12}$$

Therefore, the selection criterion of the regularization parameter ensures that the modal parameter in the identified damage state corresponding to β satisfies the following

$$Var(D) = E\left[\left\|\frac{\{R^E\} - \{R_\beta(p)\}}{\{R_\beta(p)\}}\right\|_2^2\right] = E[\,\|\delta\mu\|_2^2] = \delta^2 \tag{13}$$

The measurement noise should be estimated in advance by using prior information or through measurements to apply the DP. The implementation process will be explained in detail and demonstrated using the following experimental examples.

3.3 Summary of the two regularization parameter selection methods

For a given damage detection problem, the corresponding objective function is first solved for different β values ranging from 0 to $i \cdot \Delta\beta$, with an increment of $\Delta\beta$. The residual norm $\|R(\{p\}) - \{R^E\}\|_2^2$ and solution norm $\|\{p\}\|_1$ are then calculated. Since the regularization parameter may differ by orders for different damage configurations, the calculation range and step size $\Delta\beta$ should be set accordingly.

For the first method presented in Section 3.1, the residual and solution norms versus the regularization parameter are plotted to determine the appropriate regularization parameter, which cause both norm values are small at the same time. If the noise information is available, the DP-based strategy can be utilized for parameter selection. The L-curve of the solution norm versus the residual norm is first used to identify a preliminary range of the regularization parameter. The DP is then applied within this possible range to select the appropriate regularization parameter. The two proposed selection strategies can be used individually to determine the appropriate regularization parameter. If they are combined, the overlapped regularization parameter can be more accurate. The flowchart of the regularization parameter selection process is shown in Fig. 1.

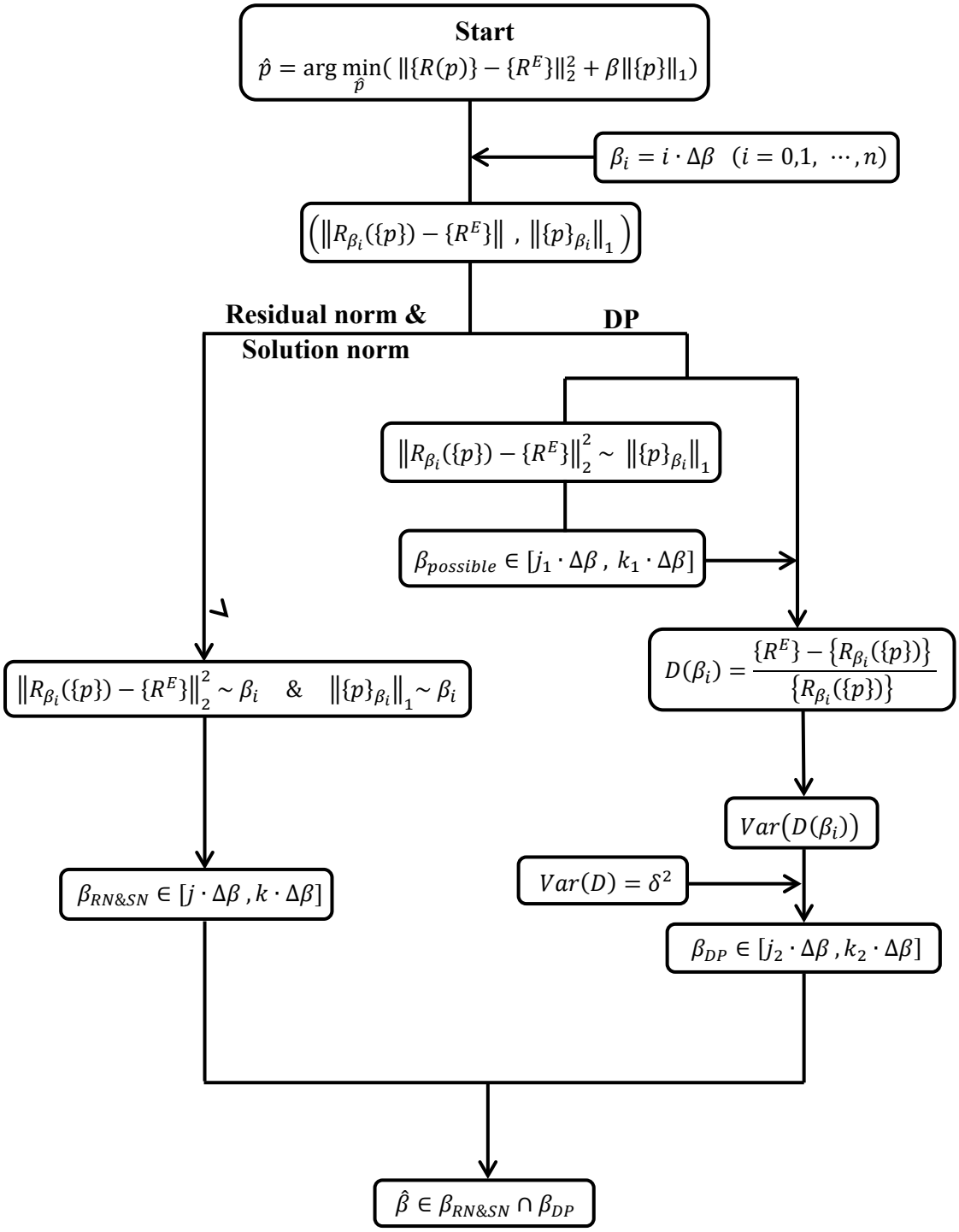

Fig. 1. Flowchart of the parameter selection process

4. A Cantilever Beam

4.1 Model descriptions

A cantilever beam (Fig. 2) is first utilized to demonstrate the effectiveness of the proposed strategies for selecting the regularization parameter. The total length of the beam is 1000 mm, and the size of the cross section is 49.60 mm ×5.0 mm. The mass density and Young's modulus are estimated as 7.67×10^{3} kg/m^{3} and 2.0×10^{11} N/m^{2}, respectively.

Fig. 2. Overview of the beam structure

4.2 Description of the experiment

A series of modal testing was conducted on the intact beam. During the laboratory test, 10 accelerometers were mounted on the beam to measure the acceleration responses to the impact force from an instrumented hammer. The measurement points were chosen every 100 mm (Fig. 3). The first six frequencies within the range of 0–300 Hz and the associated mode shapes were extracted using rational fraction polynomial method [46]. The results are listed in Table 1.

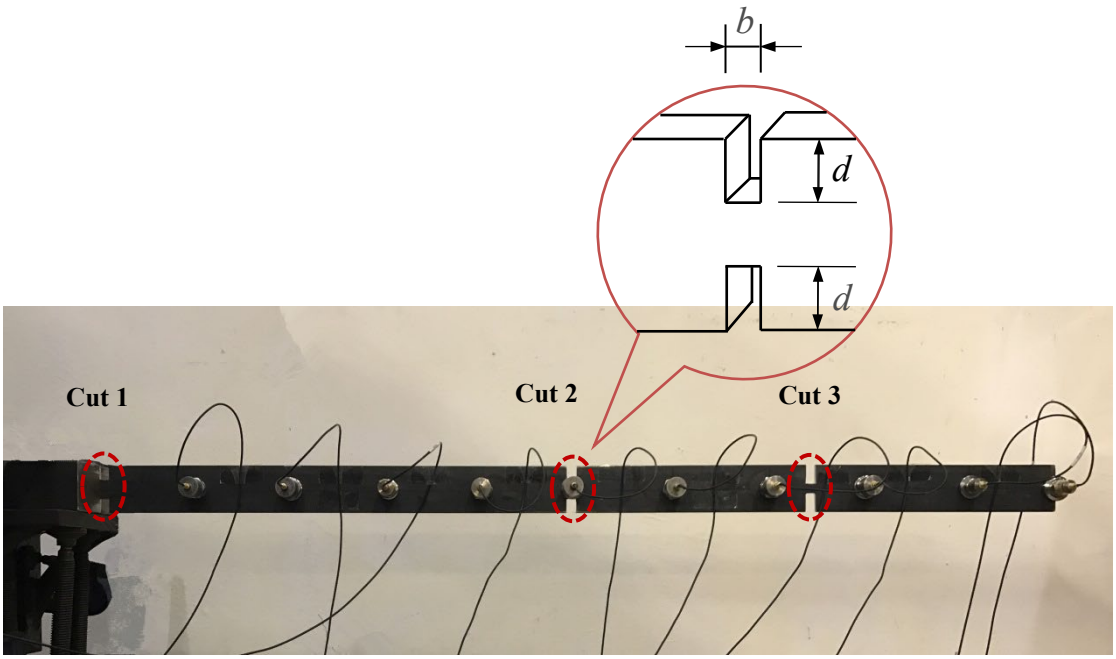

Fig. 3. Locations of accelerometers and simulated damage

Three saw cuts were sequentially introduced into the beam model (Fig. 3). The cuts have the same length b = 10 mm but varied depth for simulating different damage severities. Cut 1 at the clamped end was introduced with a depth of d = 10 mm (damage scenario 1, or DS1), representing 40% damage in the element. The depth of cut 1 was then increased to d = 15 mm (DS2). Cuts 2 and 3 were successively introduced with depth d = 15 (DS3) and 20 mm (DS4), respectively. The modal testing procedures were repeated for each damage scenario. The frequencies and mode shapes of the damaged states were extracted accordingly and listed in Table 1, in which MAC stands for modal assurance criterion indicating the similarity between two sets of mode shapes [47]. The natural frequencies experience more significant changes compared with the mode shapes. The maximum averaged change in frequencies is 8.04% with the accumulation of damage, whereas the mode shapes almost remain unchanged, especially for the first four modes.

Table 1. Measured modal data of the beam in the undamaged and damaged states

Mode no.	Undamaged	Damage scenario 1 (DS1)		Damage scenario 2 (DS2)		Damage scenario 3 (DS3)		Damage scenario 4 (DS4)	
	Freq. (Hz)	Freq. (Hz)	MAC	Freq. (Hz)	MAC	Freq. (Hz)	MAC	Freq. (Hz)	MAC
1	3.53	3.49 (−1.24)	99.99	3.38 (−4.41)	99.97	3.33 (−5.91)	99.98	3.36 (−4.91)	99.99
2	21.77	21.39 (−1.72)	99.95	20.85 (−4.26)	99.84	20.29 (−6.81)	99.86	19.76 (−9.22)	99.95
3	60.78	59.46 (−2.16)	99.88	58.93 (−3.04)	99.83	58.38 (−3.95)	99.57	54.37 (−10.55)	99.60
4	119.46	118.31 (−0.96)	99.88	116.01 (−2.88)	99.51	113.35 (−5.12)	99.23	106.31 (−11.01)	99.06
5	194.78	191.98 (−1.44)	99.78	188.74 (−3.10)	99.17	188.46 (−3.25)	98.87	187.17 (−3.91)	99.14
6	292.82	281.56 (−3.84)	98.07	286.76 (−2.07)	94.95	275.08 (−6.06)	98.26	267.45 (−8.66)	97.26
Average (%)		(−1.90)	99.59	(−3.29)	98.88	(−5.18)	99.30	(−8.04)	99.17

Note: Values in parentheses are the frequency change ratios (%) between the damaged and undamaged states

4.3 Finite element modeling of the beam

The beam is modeled using 100 Euler–Bernoulli beam elements (10 mm long). The length of one element is identical to the length of each cut; as such, the damage severity of each cut is equal to the reduction in the moment of inertia of the cross section and is quantified by SRF. The actual damage locations and severities of the four damage scenarios are listed in Table 2. Using this FE model, the first 6 modal frequencies and mode shapes are calculated and compared with the measured ones in Table 3. The averaged frequency difference is 0.54% and MAC value is 99.81, indicating that the model predictions agree well with the experimental data.

Table 2. Damage locations and severities for four damage scenarios

Scenario	Element no.	Damage severity (SRF)
DS1	1	−40%
DS2	1	−60%
DS3	1	−60%
	50	−60%
DS4	1	−60%
	50	−60%
	75	−80%

Table 3. Numerical modal data of the beam in the intact state

Mode no.	Experiment Freq. (Hz)	FE analysis					
		Initial Model			Updated Model		
		Freq. (Hz)	Diff. (%)	MAC (%)	Freq. (Hz)	Diff. (%)	MAC (%)
1	3.53	3.53	0.00	99.99	3.53	0.02	99.99
2	21.77	21.92	0.69	99.93	21.75	−0.12	99.94
3	60.78	61.22	0.72	99.71	60.67	−0.17	99.80
4	119.46	118.40	−0.89	99.76	119.21	−0.21	99.78
5	194.78	195.34	0.29	99.66	195.01	0.12	99.89
6	292.82	294.77	0.67	99.81	293.75	0.03	99.93
Average of absolute values			0.54	99.81		0.11	99.89

Among the total 100 elements of the beam model, only 1 to 3 damaged elements have non-zero SRF values. Therefore, the SRF vector is very sparse. Only the first six frequencies and mode shapes are utilized for damage detection, and 66 measurement data are obtained. Identification is an underdetermined problem because 100 unknown SRF values have to be identified. With consideration of the modeling uncertainties of the initial FE model, the FE model is first updated using the modal data measured from the undamaged state. The updated FE model matches the measurement better as the averaged frequency difference decreases from 0.54% to 0.11% and MAC increases slightly (Table 3). This updated model will be used for damage detection.

4.4 Selection of the regularization parameter

1) Damage scenario DS1

For DS1, the objective function, i.e., Eq. (6), is solved for different β values ranging from 0 to 1.0, with an increment of $\Delta\beta = 0.005$. The residual and solution norms versus β are plotted in Fig. 4. With increasing β, the solution norm drops quickly first, then decreases slowly, and suddenly drops to zero when β reaches the maximal regularization parameter $\beta_{\max} = 0.485$. The residual norm rises rapidly at the beginning and increases gradually from $\beta = 0.025$. The corresponding residual and solution norms change slowly with increasing β ($\beta = 0.06$~0.485). The regularization parameter in this range achieves a fair balance in keeping both norms small. Therefore, $\beta = 0.06$~0.485 is determined as the appropriate range of the regularization parameter.

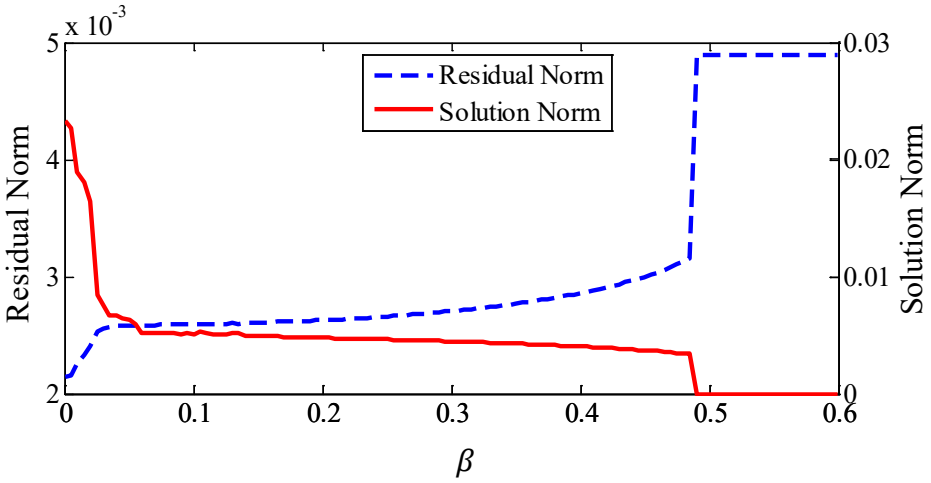

Fig. 4. Residual and solution norms for different values of β in DS1

The DP is also applied to select the regularization parameter. First, a possible range of the proper regularization parameter is determined based on the plot of the solution norm versus the residual norm on the linear scale. The variance of the discrepancy between the calculated and measured modal data is calculated over this possible range.

Natural frequencies can be measured more accurately than other vibration properties. Previous studies [43, 48-50] suggested that natural frequencies may contain 1% noise in practical vibration tests. In the present study, natural frequencies are assumed to contain 1% noise, that is, the standard deviation of noise $\delta = 0.01$. For each regularization parameter β, the corresponding discrepancy of natural frequencies can be calculated as follows

$$D(\beta) = \frac{\{f^E\} - \{f_\beta(p)\}}{\{f_\beta(p)\}} \tag{14}$$

where $\{f^E\}$ is the measured natural frequency, and $\{f_\beta(p)\}$ is the calculated natural frequencies of the damaged structure corresponding to β. According to Eq. (14), the regularization parameter is selected such that the variance of the discrepancy $Var(D(\beta))$ is closest to the estimated $\delta^2 = 1\times10^{-4}$.

The solution norm versus the residual norm for DS1 is plotted on the linear scale in Fig. 5 (a). The enlarged diagram with β within the range of 0.025–0.485 is shown in Fig. 5 (b). Although this curve has some resemblance to "L", it bunches up at some points. Therefore, it is difficult to identify the optimal regularization parameter by locating the "corner", as the L-curve criterion used in the l_2-regularized problems. Instead, a possible range of β, which is around the corner of the L-shaped curve, can be determined. For DS1, the possible range of the regularization parameter is approximately 0.025–0.485.

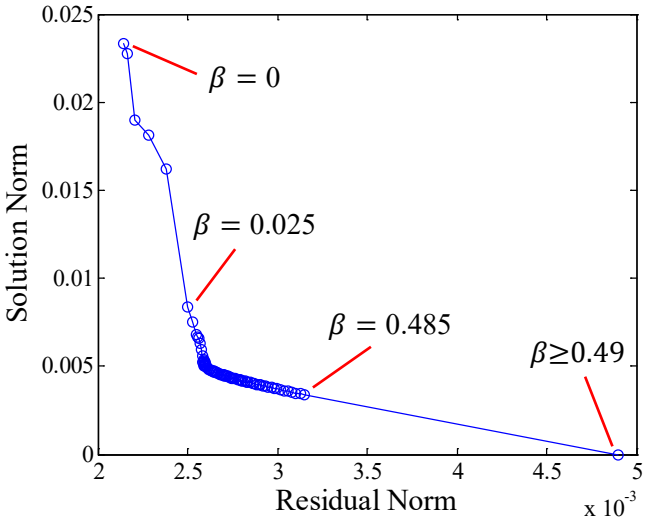

(a) β between 0 and 1

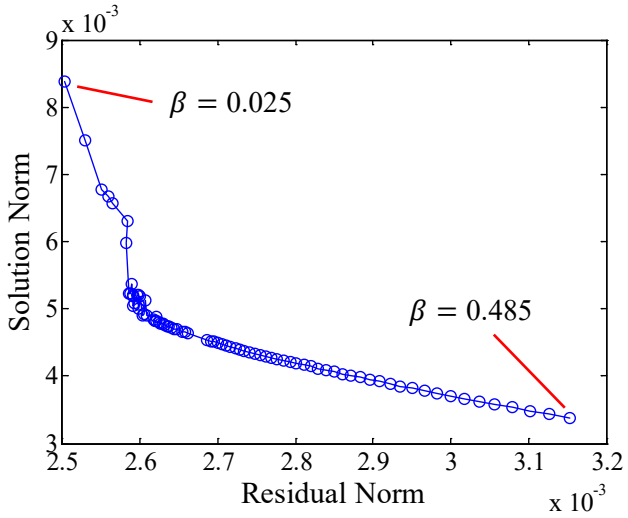

(b) β between 0.025 and 0.485

Fig. 5. Solution norm versus residual norm for a range of β between 0 and 1 (DS1)

Fig. 6 shows the $Var(D(\beta))$ for different values of β within the range of 0.025–0.485. The variances in the possible range of β are all higher than the estimated value and vary slightly. Therefore, $\beta = 0.025$~0.485 is determined as the appropriate range of the regularization parameter because the variances in this range are all close to 1×10^{-4}. The feasible ranges of the regularization parameter determined by the two proposed strategies are almost the same.

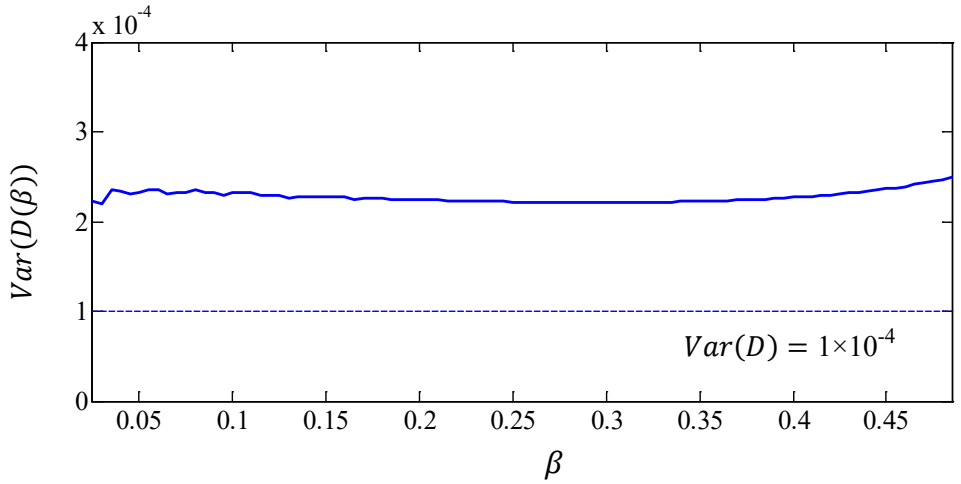

Fig. 6. $Var(D(\beta))$ for different values of β between 0.025 and 0.485 (DS1)

The damage identification results of SRFs are displayed in Fig. 7 for different values of β. For $\beta = 0.01$, although the true damage at element 1 can be detected, the identified SRFs are distributed among a number of elements. When the regularization parameter is within 0.025–0.485, the damage identification results are accurate. At $\beta = 0.025$, although several elements are falsely identified as damaged, the identified SRFs are very small and can be neglected. For the other three regularization parameters, the identified damage severities are all close to the true value (SRF_1=–0.4), and no false identification occurs. At $\beta > 0.485$, the solution becomes zero, and no damage can be detected.

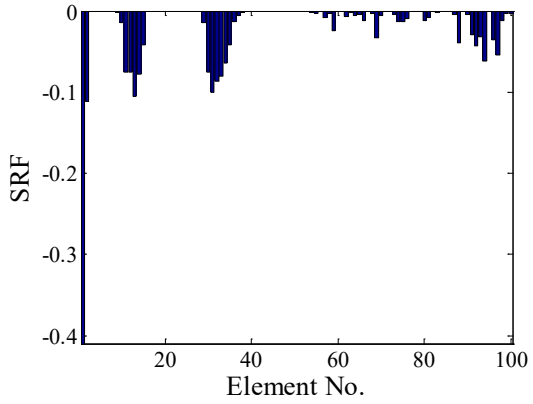

(a) $\beta = 0.01$

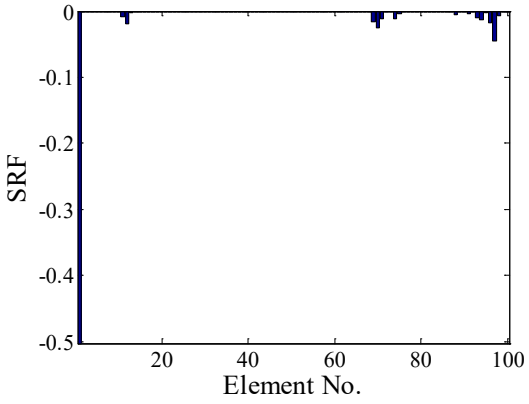

(b) $\beta = 0.025$

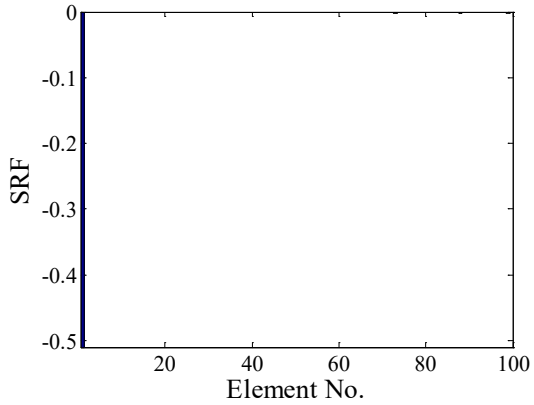

(c) $\beta = 0.06$

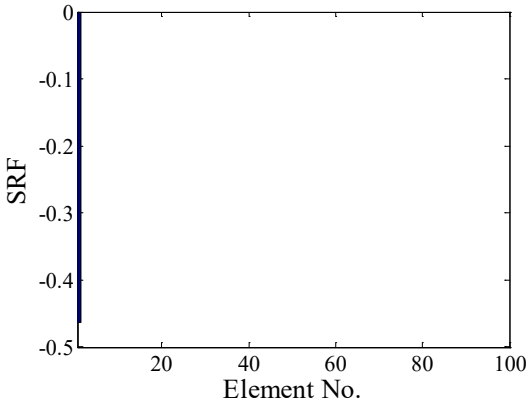

(d) $\beta = 0.25$

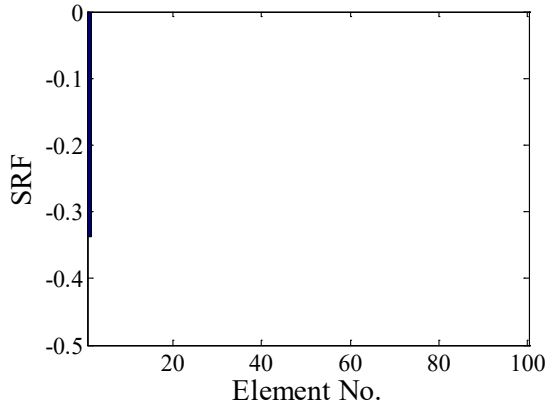

(e) $\beta = 0.485$

Fig. 7. Damage identification results for DS1

2) Damage scenario DS2

For DS2, the objective function is similarly solved for different β values ranging from 0 to 1.0 with an increment $\Delta\beta = 0.005$. The curves of the residual and solution norms versus β are shown in Fig. 8. At $\beta \geq 0.085$, the residual and solution norms are almost unchanged with increasing β. Therefore, the appropriate range of the regularization parameter is determined as $\beta = 0.085$~0.95, which keeps the two norms small at the same time.

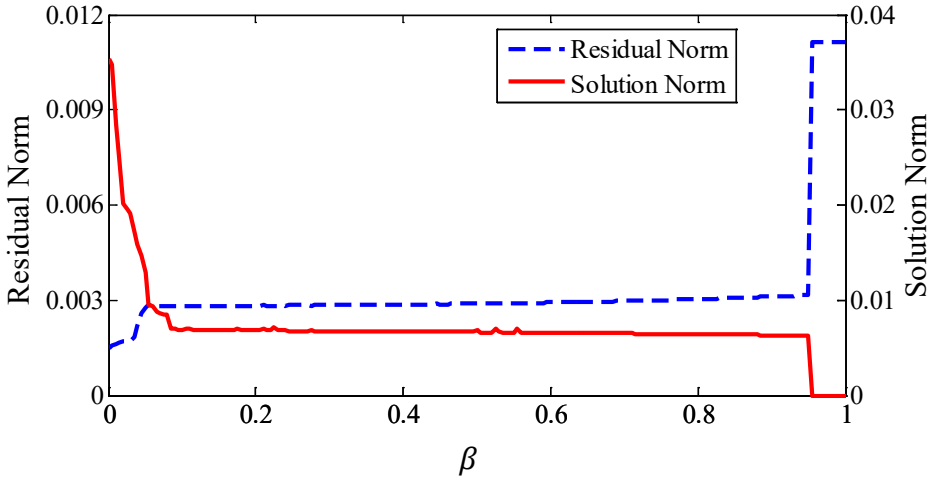

Fig. 8. Residual norm and solution norm for different values of β in DS2

The curve of the solution norm versus the residual norm on the linear scale is shown in Fig. 9. The suitable range of the regularization parameter for DS2 is first estimated as 0.055–0.95. $Var\big(D(\beta)\big)$ for different values of β in the previously mentioned range are displayed in Fig. 10. The variances vary slightly with increasing β and are all lower than the estimated value. Therefore, $\beta = 0.055$~0.95 is determined as the appropriate range of the regularization parameter with the calculated variances close to 1×10^{-4}. This range is slightly wider than that determined using the previous strategy. The damage identification results for different values of β within the range of 0.055 to 0.95 are shown in Fig. 11. In all cases, the damage location and severity are

identified accurately. When β is out of the range, the damage identification results are incorrect and not shown here for brevity.

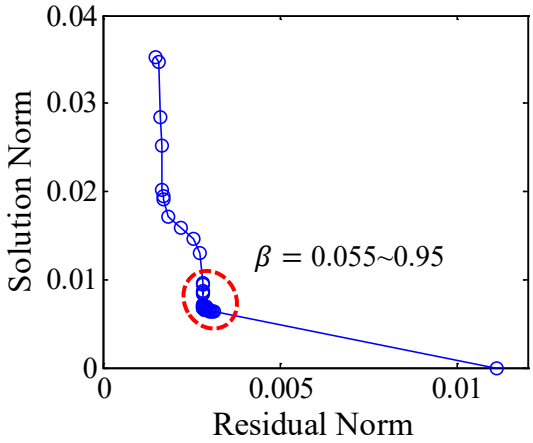

Fig. 9. Solution norm versus residual norm for a range of β between 0 and 1

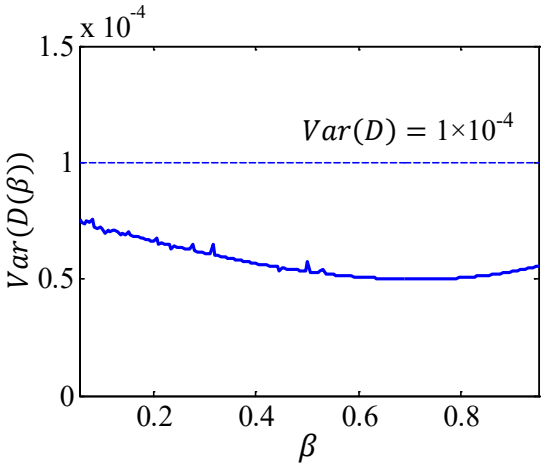

Fig. 10. $Var(D(\beta))$ for different values of β between 0.055 and 0.95 (DS2)

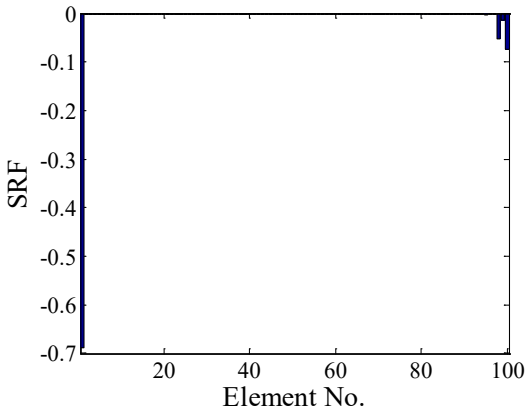

(a) $\beta = 0.055$

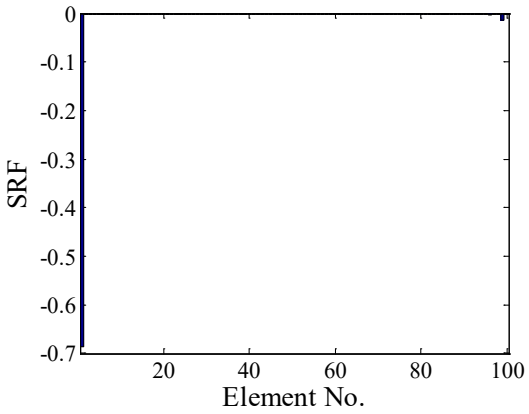

(b) $\beta = 0.085$

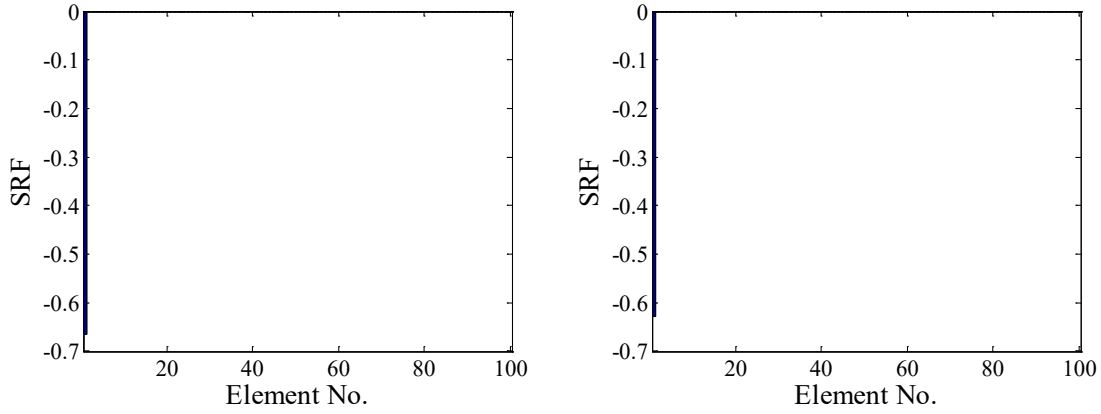

(c) $\beta = 0.49$ (d) $\beta = 0.95$

Fig. 11. Damage identification results for DS2

3) Damage scenario DS3

For DS3, the objective function is solved for different values of β ranging from 0 to 1.4 with the increment $\Delta\beta = 0.005$. The curves of the residual and solution norms versus β are displayed in Fig. 12. The residual and solution norms are almost unchanged when β is within 0.035–0.095. At $\beta > 0.095$, the residual norm increases suddenly, whereas the solution norm decreases. With increasing β, the residual and solution norms are nearly constant until the maximal regularization parameter is reached. As introduced previously, it is usually the case that the sparsity of the solution increases with increasing regularization parameter, leading to loss of data fidelity. Therefore, the appropriate range of the regularization parameter is determined as $\beta = 0.035\sim0.095$, because of minimal improvement gained by increasing the regularization parameter. This range is smaller than those of the previous two damage scenarios, indicating that the inverse problem corresponding to DS3 is more sensitive to the regularization parameter.

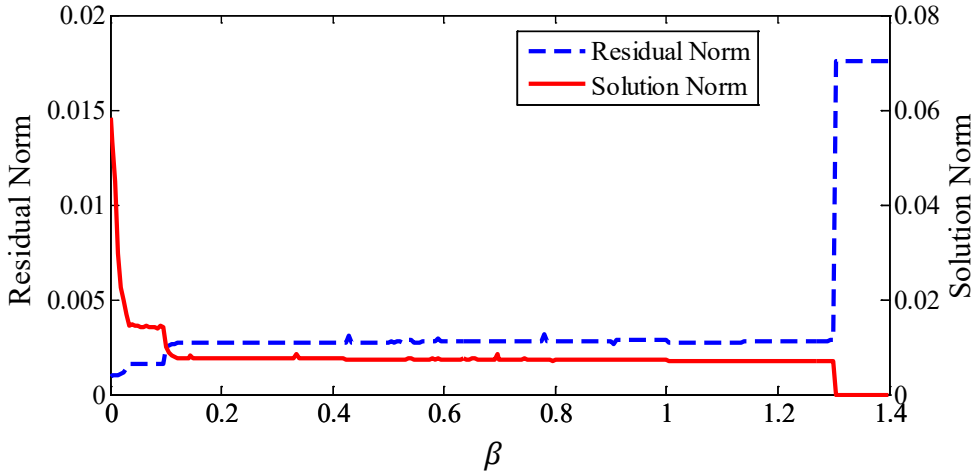

Fig. 12. Residual norm and solution norm for different values of β in DS3

The L-curve of the solution norm versus the residual norm for DS3 is shown in Fig. 13. The suitable range of the regularization parameter is estimated as 0.035~1.30. $Var(D(\beta))$ for different β values within the range are displayed in Fig. 14. The distribution of the variances exhibits a step-like pattern. The variances for $\beta \in (0.035\sim0.095)$ are very close to the estimated value (i.e., 1×10^{-4}), whereas a big and abrupt increase occurs at $\beta = 0.10$. Therefore, 0.035~0.095 is determined as the suitable range of the regularization parameter, consistent with the result obtained using the previously discussed method.

The damage identification results are displayed in Fig. 15. For $\beta = 0.035$ and $\beta = 0.095$, both damaged elements can be located and quantified correctly. At $\beta = 0.10$, the damaged elements can be detected, but the severity of the damage at the mid-span is incorrect. For $\beta = 0.80$, the damage at the mid-span of the beam cannot be identified.

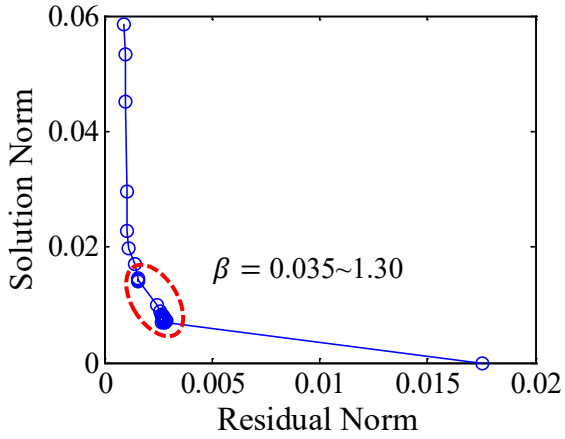

Fig. 13. Solution norm versus residual norm for a range of β between 0 and 1.4

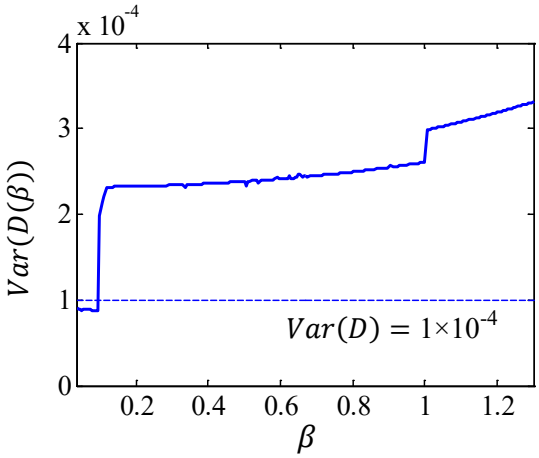

Fig. 14. $Var(D(\beta))$ for different values of β between 0.035 and 1.30 (DS3)

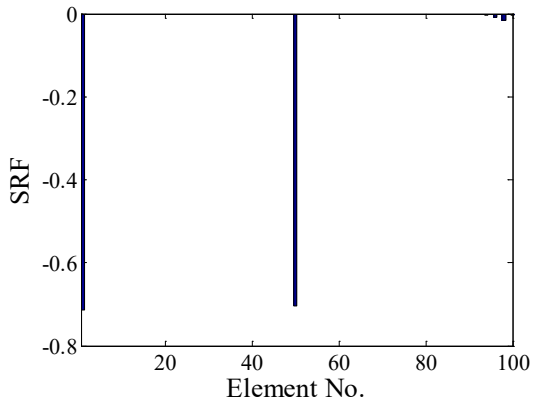

(a) β = 0.035

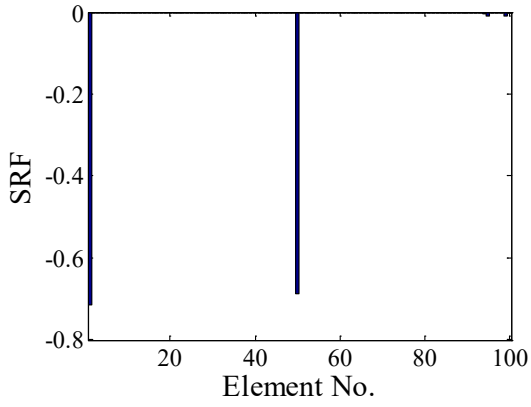

(b) β = 0.095

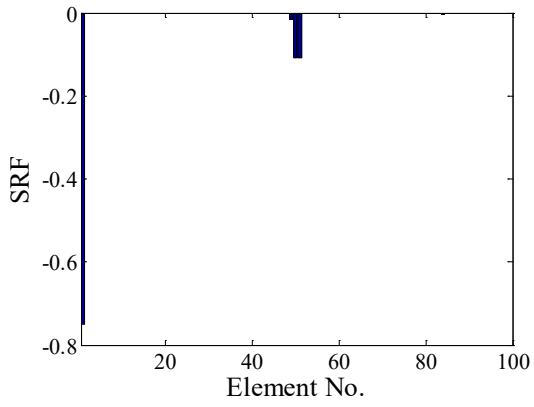

(c) β = 0.10

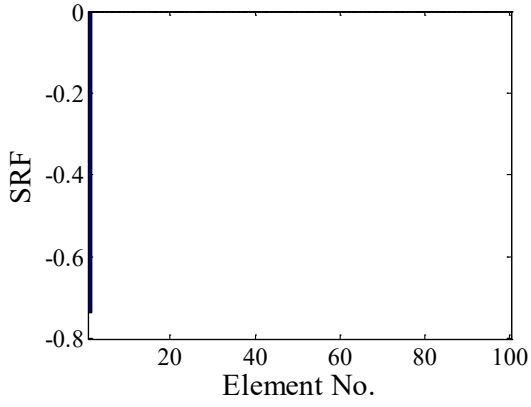

(d) β = 0.80

Fig. 15. Damage identification results for DS3

4) Damage scenario DS4

For DS4, the objective function is solved for different β values ranging from 0 to 2.2 with the increment $\Delta\beta = 0.005$. The plots of residual and solution norms versus β are shown in Fig. 16. The appropriate range of the regularization parameter is determined as $\beta = 0.095$~0.145, which keeps both the residual and solution norms small at the same time.

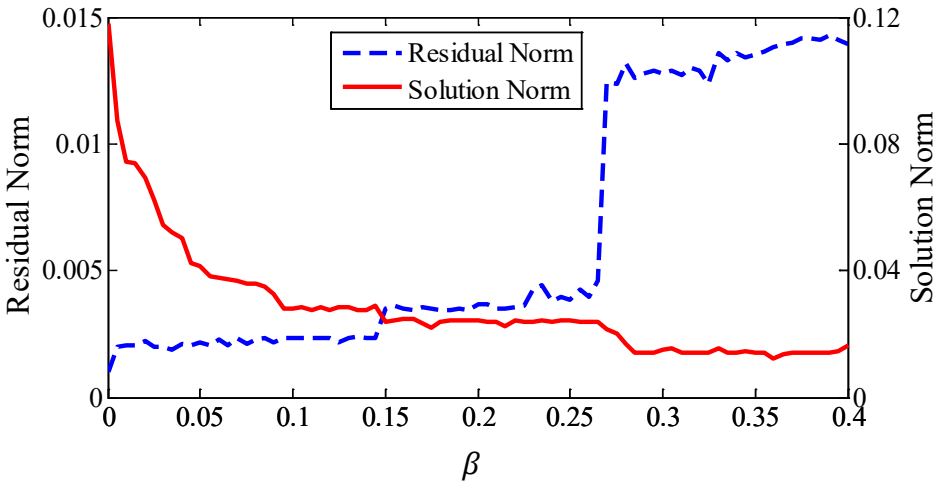

Fig. 16. Residual and solution norms for different values of β in DS4

The resulting curve of the solution norm versus the residual norm on the linear scale is shown in Fig. 17. The suitable range of the regularization parameter for DS4 is estimated as 0.095–0.30. $Var(D(\beta))$ for different values of β in the possible range are displayed in Fig. 18. The corresponding variances are all close to the estimated value at $\beta < 0.15$. Thus, the appropriate range of the regularization parameter is $\beta =$ 0.095~0.145, consistent with the result of previous strategy.

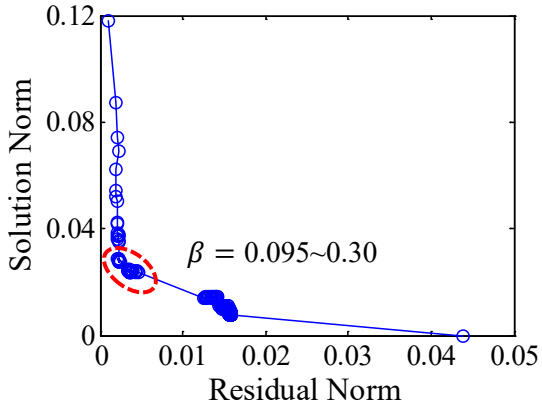

Fig. 17. Solution norm versus residual norm for a range of β between 0 and 2.2

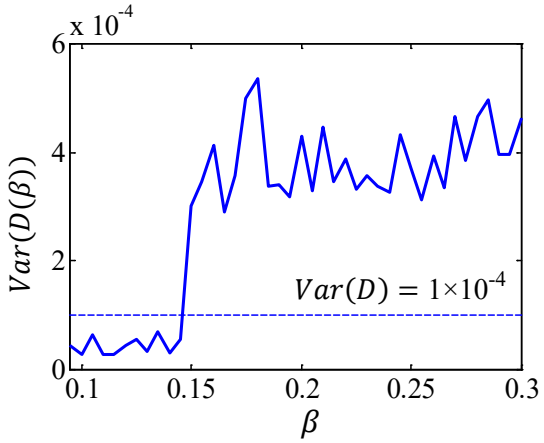

Fig. 18. $Var(D(\beta))$ for different values of β between 0.095 and 0.30 (DS4)

The damage identification results for different values of β are shown in Fig. 19. At $\beta = 0.03$, the identification result is not sparse, and a considerable number of undamaged elements are falsely identified as damaged. For $\beta = 0.095$ and $\beta = 0.145$, the damaged elements (nos. 1, 50, and 75) are located and quantified accurately. At $\beta = 0.18$, the damage in the mid-span (no. 50) cannot be detected.

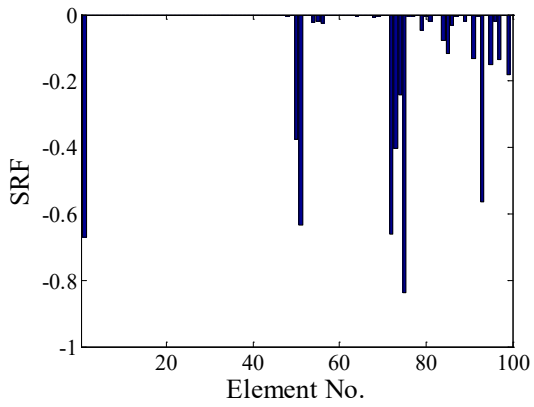

(a) $\beta = 0.03$

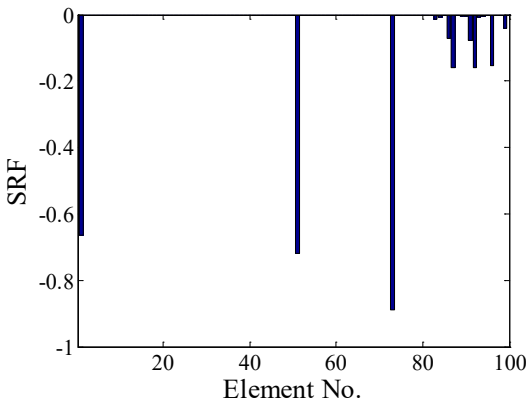

(b) $\beta = 0.095$

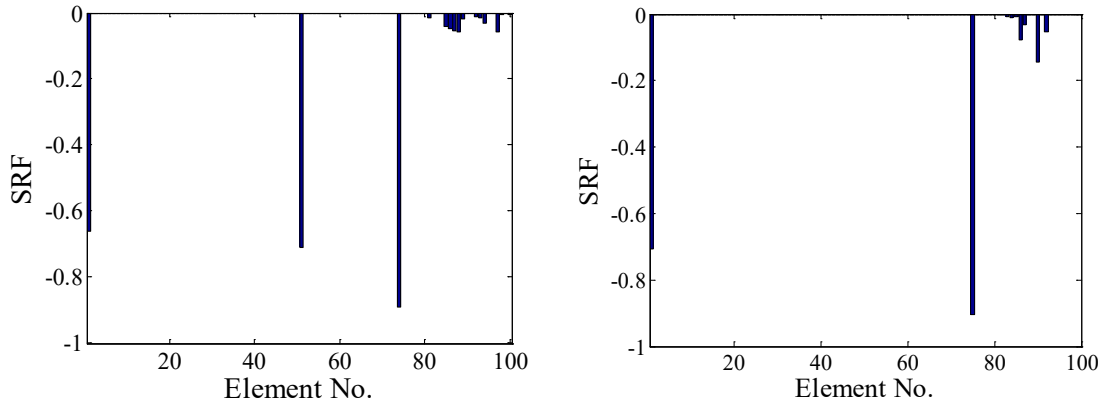

(c) $\beta = 0.145$ (d) $\beta = 0.18$

Fig. 19. Damage identification results for DS4

The experimental results show that the proposed selection strategies can provide a feasible range of the appropriate regularization parameter. The appropriate ranges determined by the two strategies are consistent with each other. Accurate damage identification results can be obtained using the regularization parameter selected from this range. Compared with single damage, multiple damage scenarios are more difficult to identify accurately. The feasible ranges of the regularization parameter for DS3 and DS4 with multiple damage are smaller than those of the two single damage scenarios. Therefore, the damage identification accuracy for multiple damage scenarios is more sensitive to the regularization parameter.

5. A Three-story Frame

5.1 Model descriptions

Hou *et al.* [13] tested a three-story steel frame (Fig. 20). Each story of the frame is 0.5 m, and the span of the beam is 0.5 m. The beams and columns have the same cross-section dimension of 75.0 mm × 5.0 mm. The mass density of the frame is 7.92×10^3 kg/m^3, and the Young's modulus is 2.0×10^{11} N/m^2. The measurement points were chosen every 100 mm, and a total of 39 measurement points were obtained. The

vertical acceleration of the beam and the horizontal acceleration of the column were measured.

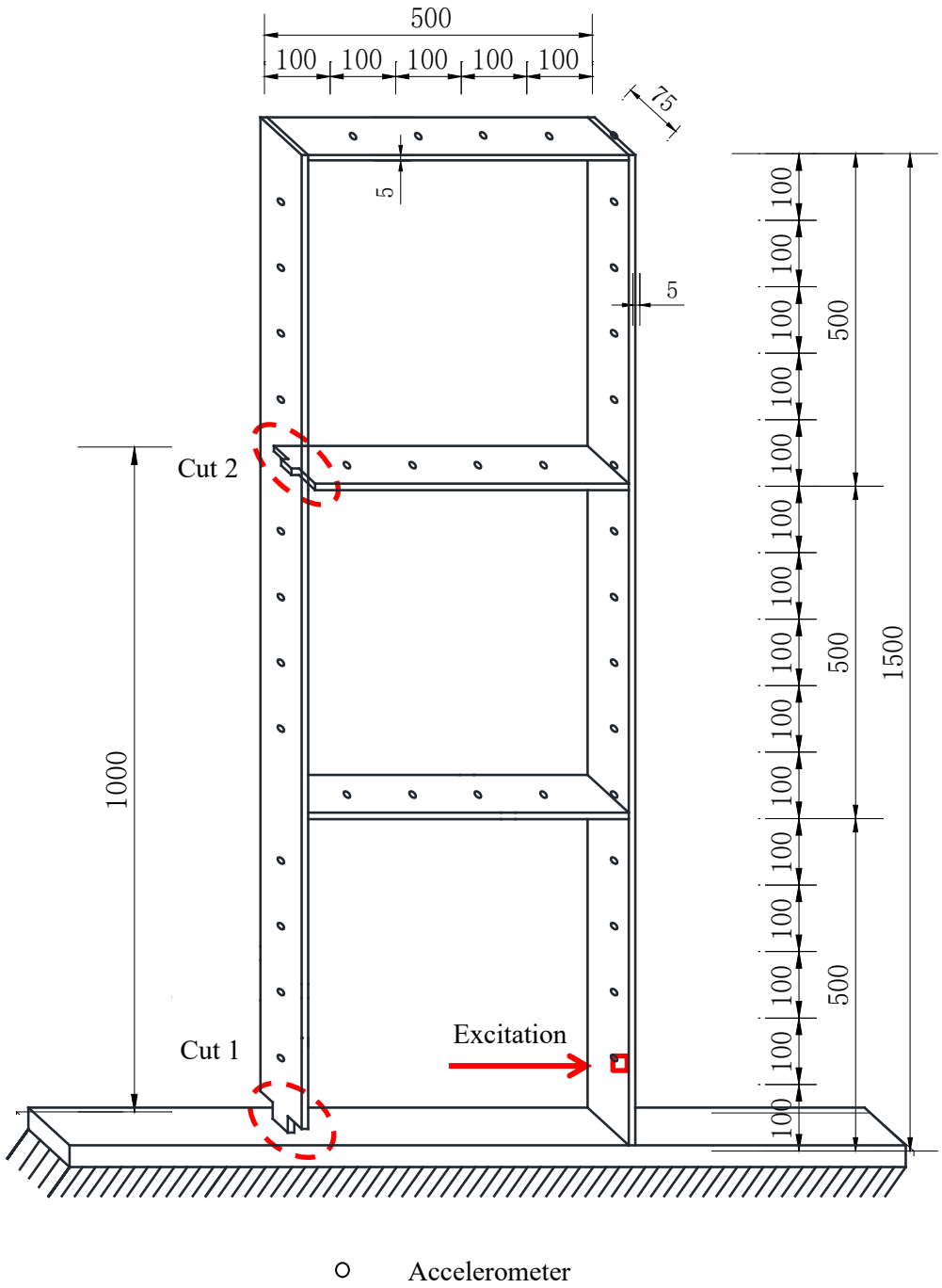

Fig. 20. Locations of accelerometers and simulated damage (Unit: mm)

Two cuts were introduced to the frame model. Cuts 1 and 2 were located at column end and the beam/column joint, corresponding to elements 1 and 176, respectively. The enlarged Cut 1 is shown in Fig. 21. The saw cuts have the same length $b = 20$ mm and depth of $d = 22.5$ mm, leading to the reduction of the moment of inertia of the cut sections by 60%, that is, SRF(1) = SRF(176) = –60%. The first eight frequencies and mode shapes of the frame structure before and after damage are listed in Table 4.

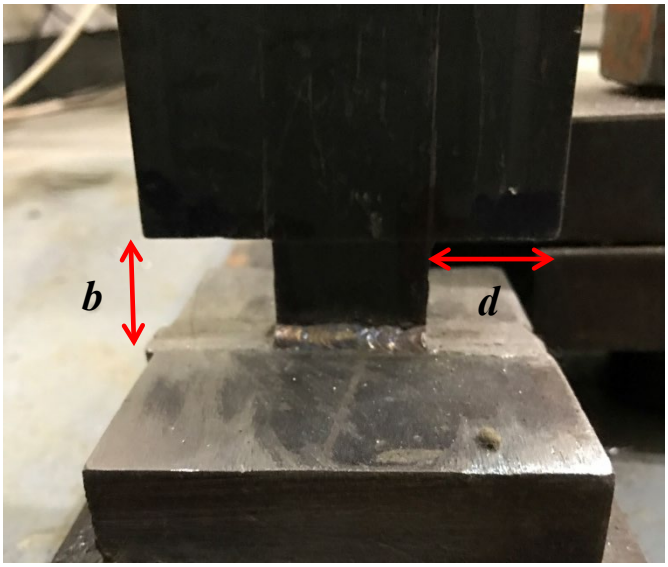

Fig. 21. Configuration of cut 1

Table 4. Measured modal data of the frame in undamaged and damaged states

Mode no.	Undamaged	Damaged	
	Freq. (Hz)	Freq. (Hz)	MAC
1	4.23	4.08 (-3.53)	95.78
2	14.03	13.45 (-4.11)	97.49
3	25.45	25.13 (-1.23)	99.01
4	44.81	44.69 (-0.27)	97.59
5	58.12	57.28 (-1.44)	91.46
6	68.36	66.11 (-3.29)	88.14
7	72.27	71.42 (-1.18)	85.80
8	91.73	88.51 (-3.52)	76.38
Average (%)		(-2.32)	91.46

5.2 Selection of the regularization parameter

In this case, the objective function is solved for different values of β ranging from 0 to 1.5 with the increment $\Delta\beta = 0.01$. The curves of the residual and solution norms versus β are shown in Fig. 22. $\beta = 0.12$~0.35 is determined as the appropriate range of the regularization parameter, where the corresponding residual and solution norms are both small.

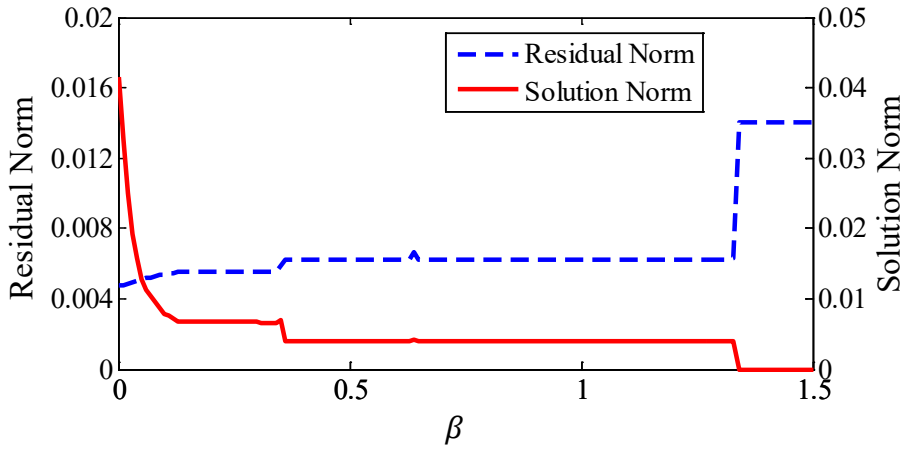

Fig. 22. Residual norm and solution norm for different values of β of the frame structure

The possible range of the optimal regularization parameter is estimated as 0.12~1.33 based on the L-curve of the residual norm versus the solution norm as displayed in Fig. 23. $Var\big(D(\beta)\big)$ for different values of β within this range are shown in Fig. 24. The variances over the possible range of β are all higher than the estimated value. With increasing β, the variance almost remains unchanged at the beginning and increases abruptly at $\beta \geq 0.36$. Therefore, $\beta = 0.12$~0.35 is chosen as the feasible range of the regularization parameter with the corresponding variances close to the estimated value. The appropriate ranges of the regularization parameter determined by the two proposed strategies are consistent.

The damage identification results for different values of β are shown in Fig. 25.

Accurate damage identification results can be obtained using the regularization parameter within 0.12–0.35. The damaged elements can be correctly detected, and no false identification occurs. At $\beta = 0.60$, which is out of the feasible range, only damage at the column end (element 1) is identified, and the other damage at element 176 is not detected.

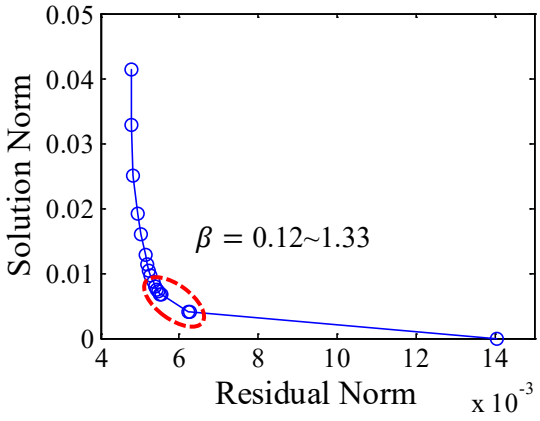

Fig. 23. Solution norm versus residual norm for a range of β between 0 and 1.5

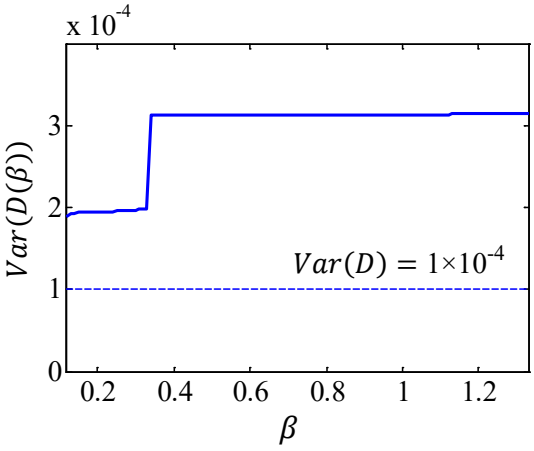

Fig. 24. $Var(D(\beta))$ for different values of β between 0.12 and 1.33 (DS4)

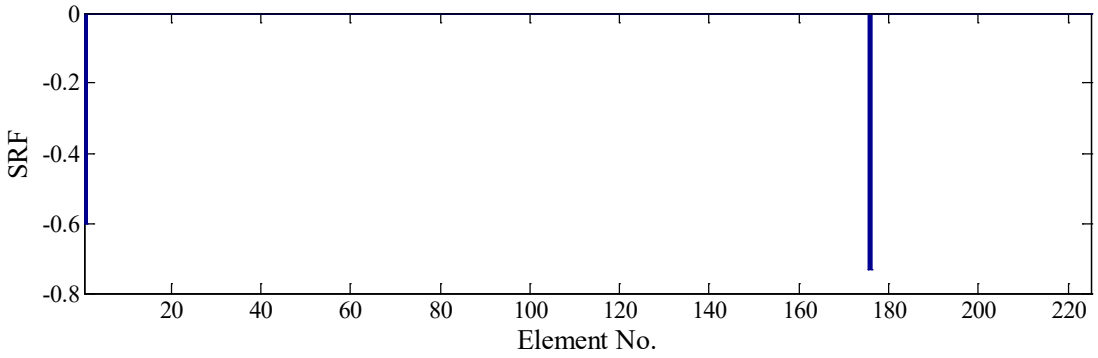

(a) $\beta = 0.12$

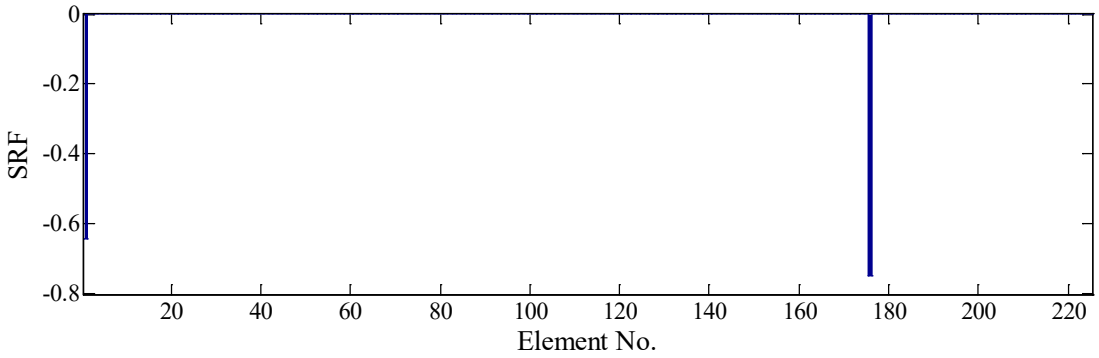

(b) $\beta = 0.20$

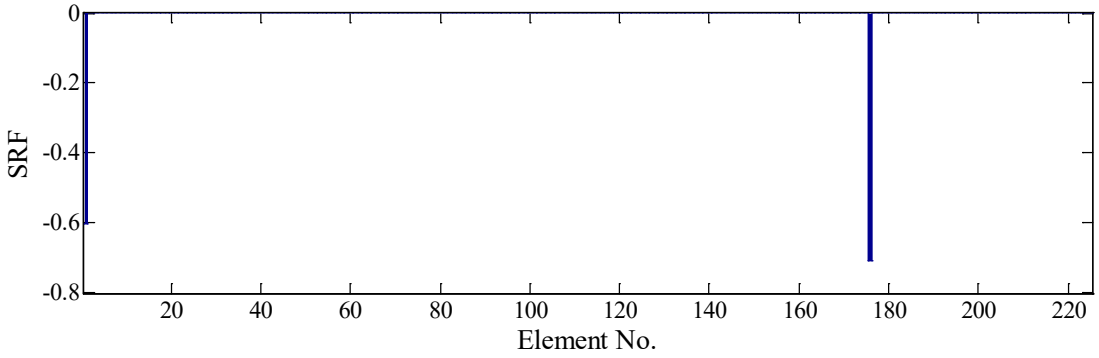

(c) $\beta = 0.35$

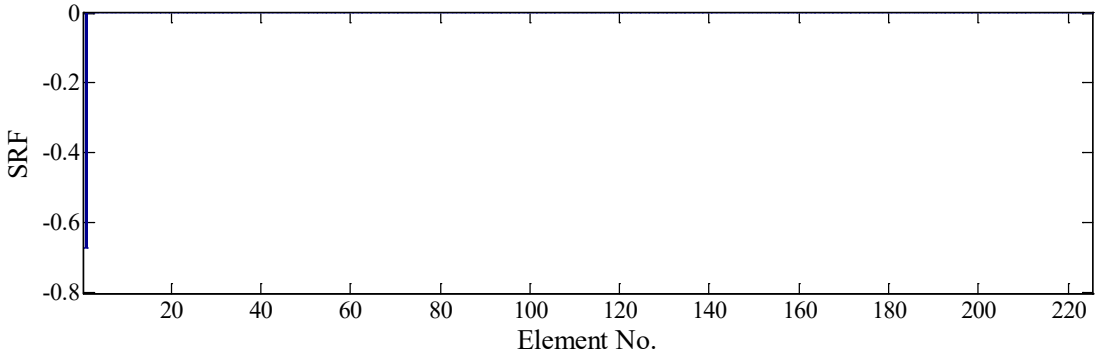

(d) $\beta = 0.60$

Fig. 25. Damage identification results for the frame structure

6. Conclusions and Discussions

Exploiting the sparse condition of structural damage, the l_1 regularization technique is employed in model updating to improve the damage identification accuracy. This study proposes two strategies for selecting the regularization parameter. Following the similar idea of the L-curve criterion for l_2 regularization, the first selection method

utilizes the residual and solution norms to determine the appropriate range of the regularization parameter. The other selection criterion is developed based on the DP such that the variance of the discrepancy between the calculated and measured modal data is close to the variance of the measurement noise.

Two experimental examples demonstrate that an appropriate range of the regularization parameter can be determined using the two proposed techniques and the results are consistent. Accurate damage identification results can be obtained when the regularization parameter is selected within the specified range even for multiple damage scenarios. When the regularization parameter is out of the range, true damage may not be detected, or undamaged elements may be falsely identified as damaged. The suitable range depends on the structure and damage scenario. A wider range indicates that the damage detection problem is insensitive to the regularization parameter.

Acknowledgements

This research was supported by the PolyU Research Grant (Project Nos. 1-ZVDN and G-YBHL) and the National Natural Science Foundation of China (Project No. 51678364).

References

1. S.W. Doebling, C.R. Farrar, M.B. Prime, D.W. Shevitz, Damage identification and health monitoring of structural and mechanical systems from changes in their vibration characteristics: a literature review, *Los Alamos National Lab. Report*, 1996.

2. J. Zhang, Y.L. Xu, Y. Xia, J. Li, A new statistical moment-nased structural damage detection method, *Struct. Eng. Mech.* 30 (4) (2008) 445-466.

3. C. Oyarzo-Vera, J. Ingham, N. Chouw, Vibration-based damage identification of an unreinforced masonry house model, *Adv. in Struct. Eng.* 20 (3) (2017) 331–351.

4. C.P. Fritzen, D. Jennewein, T. Kiefer, Damage detection based on model updating methods, *Mech. Syst. Signal Process.* 12 (1) (1998) 163-186.

5. W.Y. He, S.Y. Zhu, Z.W. Chen, Wavelet-based multi-scale finite element modeling and modal identification for structural damage detection, *Adv. in Struct. Eng.* 20 (8) (2017) 1185–1195.

6. J.T. Kim, N. Stubbs, Crack detection in beam-type structures using frequency data, *J. Sound Vib.* 259 (1) (2003) 145-160.

7. Z. Shi, S. Law, L. Zhang, Damage localization by directly using incomplete mode shapes, *J. Eng. Mech.* 126 (6) (2000) 656-660.

8. H.W. Engl, M. Hanke, A. Neubauer, *Regularization of inverse problems*, Kluwer, Dordrecht, 1996.

9. X. Li, S.S. Law, Adaptive Tikhonov regularization for damage detection based on nonlinear model updating, *Mech. Syst. Signal Process.* 24 (6) (2010) 1646-1664.

10. B. Weber, P. Paultre, J. Proulx, Structural damage detection using nonlinear parameter identification with Tikhonov regularization, *Struct. Control Health Monit.* 14 (3) (2007) 406-427.

11. X.Q. Zhou, Y. Xia, S. Weng, L_1 regularization approach to structural damage detection using frequency data, *Struct. Health Monit.* 14 (6) (2015) 571-58.

12. C. Zhang, Y. Xu, Comparative studies on damage identification with Tikhonov regularization and sparse regularization, *Struct. Control Health Monit.* 23 (3) (2016) 560-579.

13. R.R. Hou, Y. Xia, X.Q. Zhou, Structural damage detection based on l_1 regularization using natural frequencies and mode shapes, *Struct. Control Health Monit.* 25 (3) (2018), e2107.

14. D. Terzopoulos, Regularization of inverse visual problems involving discontinuities, *IEEE Trans. Pattern Anal. and Mach. Intell.* (4) (1986) 413-424.

15. S. Theodoridis, Y. Kopsinis, K Slavakis, *Sparsity-aware learning and compressed sensing: An overview*, Acad. Press Libr. Singnal Process., 2013, pp. 1271-1377.

16. H.L. Taylor, S.C. Banks, J.F. McCoy, Deconvolution with the l_1 norm, *Geophys.* 44 (1) (1979) 39-52.

17. E.J. Candès, Compressive sampling, in: *Proceedings of the international congress of mathematicians*, Madrid, Spain, 2006, pp. 1433-1452.

18. R.G. Baraniuk, More is less: signal processing and the data deluge, *Science*, 331 (6018) (2011) 717-719.

19. Y. Wang, H. Hao, An introduction to compressive sensing and its potential applications in structural engineering, *The 11th International Symposium on Structural Engineering*, Guangzhou, China, 18–20 December 2010, pp. 1089–1094.

20. Y. Wang, H. Hao, Damage identification scheme based on compressive sensing, J. Comput. Civil Eng. 29 (2) (2014) 04014037.

21. Y. Bao, H. Li, J. Ou, Emerging data technology in structural health monitoring: compressive sensing technology, *J. Civil Struct. Health Monit.* 2 (4) (2014) 77-90.

22. Y. Yang, S. Nagarajaiah, Blind denoising of structural vibration responses with outliers via principal component pursuit, *Struct. Control Health Monit.* 21 (6) (2014) 962-978.

23. S. Zhou, Y. Bao, H. Li, Structural damage identification based on substructure sensitivity and l_1 sparse regularization, *Civil Structural Health Monitoring Workshop (CSHM-4)*, San Diego, California USA, 12–15 March 2013.

24. C. Zhang, J.Z. Huang, G.Q. Song, L. Chen, Structural damage identification by extended Kalman filter with l_1-norm regularization scheme, *Struct. Control Health Monit.* 2017.

25. P.C. Hansen, The L-curve and its use in the numerical treatment of inverse problems, in: P. Johnston, editor, *Computational inverse problems in electrocardiology*, Southampton: WIT Press, 2001, pp. 119–142.

26. D.L. Phillips, A technique for the numerical solution of certain integral equations of the first kind, *J. Assoc. Comput. Mach.* 9 (1962) 84-97.

27. V.A. Morozov, On the solution of functional equations by the method of regularization, *Soviet Math. Dokl*. 7 (1966) 414-417.

28. V.A. Morozov, *Methods for solving incorrectly posed problems*, Springer Verlag, New York, 2012.

29. G.H. Golub, M. Heath, G. Wahba, Generalized cross-validation as a method for choosing a good ridge parameter, *Technometrics* 21 (2) (1979) 215-223.

30. S. Mallat, *A wavelet tour of signal processing*, Academic press, 1999.

31. I.M. Johnstone, On minimax estimation of a sparse normal mean vector, *The Ann. Stat.* (1994) 271-289.

32. F. Bauer, M.A. Lukas, Comparingparameter choice methods for regularization of ill-posed problems, *Math. Comput. Simulat.* 81 (9) (2011) 1795-1841.

33. P.C. Hansen, Analysis of discrete ill-posed problems by means of the L-curve, *SIAM Rev.* 34 (4) (1992) 561-580.

34. D. Mascarenas, A. Cattaneo, J. Theiler, C. Farrar, Compressed sensing techniques for detecting damage in structures, *Struct. Health Monit*. 12 (2013) 325-38.

35. Y. Yang, S. Nagarajaiah, Output-only modal identification by compressed sensing: Non-uniform low-rate random sampling, *Mech. Syst. Signal Process.* 56 (2015) 15-34.

36. Y. Yang, S. Nagarajaiah, Structural damage identification via a combination of blind feature extraction and sparse representation classification, *Mech. Syst. Signal Process.* 45 (1) (2014) 1-23.

37. H. Yao, P. Gerstoft, P.M. Shearer, C. Mecklenbräuker, Compressive sensing of the Tohoku-Oki Mw 9.0 earthquake: Frequency-dependent rupture modes, *Geophy. Res. Lett.* 38 (20) (2011).

38. Y.L. Xu, J. Zhang, J.C. Li, Y. Xia, Experimental investigation on statistical

moment-based structural damage detection method, *Struct. Health Monit*. 8 (6) (2009) 555-571.

39. K. Koh, S.J. Kim, S. Boyd, An interior-point method for large-scale l_1-regularized logistic regression, *J. Mach. Learn. Res.* 8 (7) (2007) 1519-1555.

40. M.A. Lukas, On the discrepancy principle and generalised maximum likelihood for regularisation, *Bull. Aust. Math. Soc.* 52 (1995) 399–424.

41. T. Raus, U. Hämarik, On the choice of the regularization parameter in ill-posed problems with approximately given noise level of data, *J. Inverse Ill-Posed Probl.* 14 (2006) 251–266.

42. J. Dong, G. Zhang, Z. Zhang, Y. Geng, J. Wang, Inverse problem solution and regularization parameter selection for current distribution reconstruction in switching arcs by inverting magnetic fields, *Math. Probl. Eng. vol.* 2018. doi:10.1155/2018/7452863

43. A. Philips Adewuyi, Z. Wu, N.H.M. Kammrujaman Serker, Assessment of vibration-based damage identification methods using displacement and distributed strain measurements, *Struct. Health Monit.* 8 (6) (2009) 443-461.

44. D. Wu, S.S. Law, Damage localization in plate structures from uniform load surface curvature, *J. Sound Vib.* 276 (1) (2004) 227-244.

45. G. Tondreau, E. Reynders, A. Deraemaeker, Towards a more realistic modelling of the uncertainty on identified mode shapes due to measurement noise, *Proceedings of the Ninth International Conference on Damage Assessment of Structures*, Oxford, UK, 2011.

46. D. Formenti, M. Richardson, Parameter estimation from frequency response measurements using rational fraction polynomials (twenty years of progress), *Proceedings of International Modal Analysis Conference*, Orlando, Florida, 2002, pp. 167-181.

47. R.J. Allemang, D.L. Brown, A correlation coefficient for modal vector analysis, *Proceedings of the 1st International Modal Analysis Conference*, Orlando, Florida, 1982, pp. 110-116.

48. S. Weng, Y. Xia, X.Q. Zhou, Y.L. Xu, H.P. Zhu, Inverse substructure method for model updating of structures, *J. Sound Vib.* 331 (25) (2012) 5449-5468.

49. J. Mottershead, M. Friswell, Model updating in structural dynamics: a survey, *J.*

Sound Vib. 167 (2) (1993) 347-375.

50. M. Friswell, J.E. Penny, The practical limits of damage detection and location using vibration data, *Proceedings of the 11th VPI and SU Symposium on Structural Dynamics and Control*, Blacksburg, Virginia, 1997, pp. 31-40.